

1 **Initiation and long-term instability of the East Antarctic Ice Sheet**

2

3 Sean P. S. Gulick<sup>1</sup>, Amelia E. Shevenell<sup>2\*</sup>, Aleksandr Montelli<sup>1†</sup>, Rodrigo Fernandez<sup>1</sup>,  
4 Catherine Smith<sup>2</sup>, Sophie Warny<sup>3</sup>, Steven M. Bohaty<sup>4</sup>, Charlotte Sjunneskog<sup>5</sup>, Amy  
5 Leventer<sup>6</sup>, Bruce Frederick<sup>1††</sup>, Donald D. Blankenship<sup>1</sup>

6

7 <sup>1</sup>Institute for Geophysics, Jackson School of Geosciences, University of Texas at Austin, Austin,  
8 Texas 78758, USA.

9

10 <sup>2</sup>College of Marine Science, University of South Florida, Saint Petersburg, Florida, 33701, USA.

11

12 <sup>3</sup>Department of Geology and Geophysics and Museum of Natural Science, Louisiana State  
13 University, Baton Rouge, Louisiana, 70803, USA.

14

15 <sup>4</sup>School of Ocean and Earth Science, University of Southampton, Southampton S0143ZH, UK.

16

17 <sup>5</sup>Antarctic Marine Geological Research Facility, Florida State University, Tallahassee, Florida,  
18 32306, USA.

19

20 <sup>6</sup>Geology Department, Colgate University, Hamilton, New York, 13346, USA.

21

22

---

\*Joint first-author.

†Present Address: Scott Polar Research Institute, University of Cambridge, Cambridge, CB2 1ER, UK.

††Present Address: Department of Geology, University of Kansas, Lawrence, Kansas, 66045, USA.

23 Continental-scale Antarctic ice sheets have evolved over the last 50 million years<sup>1-4</sup>.  
24 However, sparse ice-proximal records<sup>5-8</sup> limit understanding of past East Antarctic  
25 Ice Sheet (EAIS) behavior and thus, our ability to evaluate its response to ongoing  
26 environmental change. The EAIS is marine-based within the Aurora Subglacial Basin  
27 (ASB), indicating that this catchment, which drains ice to the Sabrina Coast, may be  
28 sensitive to climate perturbations<sup>9-11</sup>. Here we show, using marine geological and  
29 geophysical data from the continental shelf seaward of the ASB, that marine-  
30 terminating glaciers existed at the Sabrina Coast by the early-to-middle Eocene. This  
31 finding implies substantial ice volume in the ASB before continental-scale marine-  
32 terminating ice sheets were established ~34 million years ago<sup>1-4</sup>. Subsequently, ice  
33 advanced and retreated from the ASB and across the continental shelf at least eleven  
34 times during the Oligocene and Miocene. Tunnel valleys<sup>12</sup> associated with half of these  
35 glaciations indicate a surface meltwater-rich sub-polar glacial system existed under  
36 climate conditions similar to those anticipated with continued anthropogenic  
37 warming<sup>10,11</sup>. Cooling since the Late Miocene<sup>13</sup> resulted in an expanded polar EAIS  
38 and a limited ASB catchment response to Pliocene warmth<sup>14-16</sup>. Geologic records  
39 indicate that atmospheric temperature and surface-derived meltwater may play  
40 important roles in Antarctic ice mass balance under warmer than present climates,  
41 with significant implications for future global sea level projections<sup>10,11,15,17</sup>.

42

43 The East Antarctic Ice Sheet (EAIS) response to anthropogenic warming and contribution  
44 to global sea level are the largest uncertainties in climate models because EAIS  
45 formation, evolution, and behavior during past warm climates are poorly understood<sup>10,11</sup>.

46 Deep-sea benthic foraminifer oxygen isotopes ( $\delta^{18}\text{O}$ ) indicate that during the early  
47 Eocene (53-51 million years ago (Ma)), Earth experienced the warmest conditions of the  
48 past 65 million years (myr)<sup>1,4,17,18</sup>. This warmth was followed by ~15 myr of cooling,  
49 declining atmospheric CO<sub>2</sub>, tectonic reorganizations, and development of continental-  
50 scale Antarctic ice sheets by the earliest Oligocene (33.6 Ma)<sup>1-4,17-19</sup>. As atmospheric CO<sub>2</sub>

51 declined through the Oligocene and Miocene, deep-sea  $\delta^{18}\text{O}$  and far-field sea level  
52 records suggest that ice sheets advanced to and retreated from Antarctica's continental  
53 shelves in response to astronomically-paced changes in solar insolation<sup>3,4,18,20,21</sup>. These  
54 records also suggest larger Antarctic ice sheets with less pronounced growth and decay  
55 cycles after the middle Miocene ( $\sim 13.8$  Ma)<sup>1,4</sup>, when global climate was cool and  
56 atmospheric  $\text{CO}_2$  concentrations low, relative to the Eocene and Oligocene<sup>4,17</sup>. While far-  
57 field records provide a general framework for understanding Cenozoic Antarctic  
58 cryosphere development, these records provide little direct evidence for ice location,  
59 extent, or thermal conditions required to assess climate forcings and feedbacks involved  
60 in Antarctic cryosphere and global climate evolution and are complicated by Northern  
61 Hemisphere ice volume in the Plio-Pleistocene<sup>1,3,4</sup>.

62

63 East Antarctic continental margin and the Southern Ocean sediments provide direct  
64 evidence of EAIS evolution, indicating regional marine-terminating ice in the late  
65 Eocene<sup>22-24</sup> and astronomically-paced glacial-interglacial cycles through the Pliocene<sup>5,6,14</sup>.  
66 However, existing ice-proximal records are geographically limited and temporally  
67 discontinuous, making regional comparisons difficult. Recent ice sheet models provide  
68 additional insight into EAIS evolution<sup>10,11,25</sup>. Outputs indicate that EAIS catchments with  
69 deep landward-dipping subglacial topography and surface meltwater, including the  
70 Aurora Subglacial Basin (ASB), may be sensitive to climate perturbations (e.g.  
71 atmospheric and/or oceanic temperatures, atmospheric  $\text{CO}_2$ , sea level)<sup>9-11,25</sup>. However,  
72 outputs depend on poorly constrained initial boundary conditions<sup>17,24,25</sup>, feedbacks<sup>18</sup>, and  
73 retreat mechanisms<sup>11</sup>. Thus, significant uncertainties remain regarding EAIS evolution

74 that can only be resolved with well-dated ice-proximal marine geologic and geophysical  
75 data<sup>1,19</sup>.

76

77 To improve predictions of future EAIS response to warming and contribution to global  
78 sea level rise<sup>10,11</sup>, knowledge of EAIS evolution in catchments with large potential sea-  
79 level contributions is critical. The low-lying glacially sculpted ASB catchment (~3-5 m  
80 sea-level equivalent ice<sup>9,15,26</sup>; Fig. 1a) drains ice from the Gamburtsev Mountains to the  
81 Sabrina Coast via the Totten Glacier, which is experiencing the largest mass loss in East  
82 Antarctica<sup>27</sup> and is influenced by warm subsurface (deeper than 400 m) ocean waters at  
83 its grounding line<sup>28</sup>. The ASB catchment consists of several over-deepened basins<sup>15,26</sup> and  
84 hosts an active subglacial hydrological system that drains basal meltwater to the ocean<sup>29</sup>,  
85 suggesting that regional outlet glaciers may be susceptible to both progressive retreat<sup>13</sup>  
86 and changing subglacial hydrology<sup>29</sup>. Thus, regional glacial dynamics and, ultimately, sea  
87 level contribution during a given warm interval depends on both catchment and glacier  
88 boundary conditions (e.g., subglacial topography, substrate, and/or meltwater  
89 presence/volume) coupled to atmospheric and oceanic forcings.

90

91 We present the first ice-proximal marine geophysical and geological records of ASB  
92 glacial evolution (Methods; Figs. 1b, 2, 3a). To document regional glacial development,  
93 ice dynamics, and the timing of significant environmental transitions, we integrate  
94 seismic reflection and sedimentary data from the Sabrina Coast continental shelf, at the  
95 outlet of the ASB (Fig. 1b). This margin formed during Late Cretaceous rifting of  
96 Antarctica and Australia, with tectonic subsidence continuing through the Paleogene<sup>8</sup>.

97 The present-day continental shelf is ~200 km wide, ~600 m deep, and slopes landward  
98 (Fig. 1b). We imaged ~1300 m of dipping sedimentary strata that overlie acoustic  
99 basement on the inner continental shelf (Methods; Fig. 1b). We identified three distinct  
100 packages of sedimentary rocks bounded by basement, regionally extensive  
101 unconformities, and the seafloor, termed Megasequences I-III (MS-I, -II, -III; Figs. 2a,  
102 2c, 3a, Extended Data Fig. 1). Glacial erosion truncated imaged reflectors at the sea floor,  
103 allowing us to recover and date strata near the top of MS-I and at the base of MS-III  
104 (Methods; Figs. 2a, 2c).

105

106 The deepest unit, MS-I, overlies basement and consists of a ~620 m thick, seaward  
107 dipping sequence of low-amplitude discontinuous reflectors that increase in amplitude  
108 and lateral continuity up-section (Methods; Fig. 2a, Extended Data Fig. 1). No evidence  
109 of glacial erosion exists within these strata (Figs. 2a, 3a, Extended Data Fig. 1). On the  
110 mid-shelf, we imaged two intervals of inclined stratal surfaces (clinoforms), indicating  
111 times of high sediment flux to an unglaciated continental margin (Fig. 2a). Piston core  
112 NPB14-02 JPC-55 (1.69 m) recovered mica-rich silty sands 15-20 m below the upper  
113 clinoform (Methods; Fig. 2a, Extended Data Figs. 1b, 2a, Extended Data Table 1).

114 Terrestrial palynomorphs and benthic foraminifers indicate that these marine sediments  
115 are late Paleocene in age (Methods; Fig. 2b, Extended Data Figs. 1, 2, 5, Extended Data  
116 Tables 2, 3), confirming the pre-glacial seismic interpretation of MS-I.

117

118 Above the upper clinoform, within MS-I, are a series of moderate- to high-amplitude,  
119 laterally variable reflectors (gray shading; Methods; Fig. 2a, Extended Data Fig. 1).

120 Piston core NBP14-02 JPC-54 (1.2 m; Methods; Fig. 2a, Extended Data Figs. 1b, 3),  
121 recovered from this interval, contains centimeter-scale limestones interpreted as ice-rafted  
122 debris (IRD). Terrestrial palynomorphs indicate that these sediments are of early-to-  
123 middle Eocene age (Methods; Fig. 2b, Extended Data Table 2). Laterally variable  
124 reflectivity without chaotic seismic facies, with IRD, and no evidence for cross-shelf  
125 glacial erosion indicate that marine-terminating glaciers were present at the Sabrina Coast  
126 by the middle Eocene, but grounded ice had not yet advanced across the shelf (Figs. 2a,  
127 3a).

128

129 MS-I strata reveal episodes of enhanced sediment flux from the ASB, followed by the  
130 early-to-middle Eocene arrival of marine-terminating glaciers to the Sabrina Coast.  
131 Models and observations indicate that Antarctica's ice sheets nucleated in the higher  
132 elevations of the Gamburtsev Mountains and first reached the ocean near the Sabrina  
133 Coast and Prydz Bay<sup>19</sup>, increasing sediment flux to the Australo-Antarctic Gulf<sup>30</sup>. Within  
134 the ASB are a series of topographically constrained basins that likely hosted  
135 progressively larger ice volumes<sup>15,26</sup> as ice expanded in the catchment (Fig. 1a). We  
136 speculate that after the early Eocene climate optimum (53-51 Ma), as regional and global  
137 temperatures cooled and atmospheric CO<sub>2</sub> declined<sup>17,18</sup> (Figs. 3b-c), glacial ice breached  
138 the northern ASB highlands<sup>26</sup>, allowing marine-terminating glaciers to deliver IRD to the  
139 Sabrina Coast shelf by the early-to-middle Eocene (Figs. 1a, 2a, Extended Data Fig. 2).  
140 This finding is significant and indicates 1) substantial East Antarctic ice volume by the  
141 early-to-middle Eocene and 2) the relatively early arrival of marine-terminating glaciers  
142 to the Sabrina Coast, compared with late Eocene arrivals in Prydz Bay and the Weddell

143 Sea<sup>22-24</sup>. Due to the relative paucity of Eocene data from Antarctica's margins, it is not  
144 clear if this early arrival is unique to the Sabrina Coast, or if equivalent data have not yet  
145 been recovered.

146

147 Up-section (~13 m) from core JPC-54, the deepest regionally mappable roughly-eroded  
148 surface (dark blue horizon; Figs. 2a, 3a, Extended Data Fig. 1) separates MS-I from MS-  
149 II strata and provides the first preserved evidence of grounded ice on the Sabrina Coast  
150 shelf (Methods). MS-II is up to 675 m thick with ten additional erosive surfaces (gray  
151 numbered horizons; Fig. 3a, ED Fig. 1) that truncate reflectors and exhibit rough  
152 morphology and/or channels indicative of glacial erosion in a meltwater-rich  
153 environment<sup>7,12,29,30</sup> (Methods). Between erosive surfaces, we observe strata with parallel  
154 high-amplitude reflectivity and prograding strata of varying thickness (Methods), which  
155 indicate open marine conditions and intervals of high sediment flux<sup>7,8</sup>, respectively,  
156 between the 11 glacial advances and retreats from the ASB.

157

158 Unlike previously imaged East Antarctic shelf sequences<sup>7,8</sup>, Sabrina Coast MS-II reveals  
159 multiple erosive surfaces (2-6, 8, 9) with U-shaped channels carved into sedimentary  
160 strata (Fig. 3a). Based upon geometry and size (Methods;  $\leq 170$  m deep;  $\sim 1150$  m wide),  
161 these channels are consistent with subglacial tunnel valleys observed in surface  
162 meltwater-rich sub-polar glacial systems<sup>12</sup>. The most significant channels are associated  
163 with surfaces 3-5, 8, and 9 (Fig. 3a, Extended Data Fig. 1e). Overlying erosive surface 11  
164 (Fig. 3a, Extended Data Fig. 1e) is a  $\sim 330$  m thick sequence of seaward dipping strata  
165 devoid of rough erosional surfaces, indicating prolonged continental shelf progradation

166 and/or high sediment flux in an open marine setting<sup>7,8</sup>. A regional landward-dipping  
167 angular unconformity truncates seaward-dipping MS-II (and in some places, MS-I) strata  
168 (light blue horizon; Figs. 2a, 2c, 3a, Extended Data Fig. 1). Late Miocene-to-earliest  
169 Pliocene diatomites were recovered from and immediately above the unconformity (Figs.  
170 2c-d, Extended Data Figs. 1, 4, 6). As we may not have recovered sediments below the  
171 unconformity, we consider the late Miocene (~7-5.5 Ma) the youngest possible age for  
172 the MS-III base (Fig. 2d).

173

174 Ice advanced across the Sabrina Coast continental shelf at least 11 times from the early-  
175 to-middle Eocene to late Miocene (Fig. 3a), when average atmospheric CO<sub>2</sub>  
176 concentrations (Fig. 3b), global temperatures (Fig. 3c), and global sea levels (Fig. 3d)  
177 were similar to or higher than present<sup>4,17,18</sup>. Without additional age constraints, the pacing  
178 of these glaciations is unknown, but far-field and ice-proximal records indicate  
179 cryosphere sensitivity to astronomically-paced insolation changes during the Oligo-  
180 Miocene<sup>5,20,21</sup>. The scale of Sabrina Coast shelf tunnel valleys and the presence of similar  
181 channels within the ASB catchment, ~400 km from the present grounding line, suggest  
182 that regional subglacial hydrologic systems were fed by large volumes of surface  
183 meltwater during Oligo-Miocene glacial-interglacial cycles (Methods)<sup>11,15</sup>. Thus, during  
184 climates similar to or warmer than present, surface-derived meltwater may play an  
185 important role in EAIS behavior<sup>29</sup>, as indicated by models<sup>11</sup>. The prograding sequence at  
186 the top of MS-II is similar to middle to late Miocene sequences in Wilkes Land and Prydz  
187 Bay, which reflect the transition from sub-polar to polar glacial regimes<sup>7,8</sup> (Fig. 3a,  
188 Extended Data Fig. 1e).



189

190 Above the regional unconformity, MS-III consists of a  $\leq 110$  veneer of sub-horizontal to  
191 landward-dipping strata that thicken landward, indicating substantial glacial erosion of  
192 MS-II and/or lower regional sediment flux and onset of ice loading by the late Miocene<sup>8</sup>  
193 (Methods; Figs. 2a, 2c, 3a, Extended Data Fig. 1). MS-III strata contain no visible  
194 channels, suggesting reduced regional surface meltwater influence and/or more diffuse  
195 basal meltwater flux<sup>12,15,26,29</sup>. High-amplitude reflectors (Fig. 3a) within acoustically  
196 chaotic MS-III strata indicate erosional surfaces in late Miocene to Pleistocene tills  
197 (Methods) and advance/retreat of an expanded EAIS<sup>15</sup>. Open marine sediments are  
198 present, but the lack of significant accumulation and/or preservation suggests limited  
199 regional ice retreat and/or shorter interglacials since the late Miocene (Methods; Figs. 2c,  
200 3a, Extended Data Fig. 1).

201

202 An expanded polar EAIS occupied the ASB catchment and Sabrina Coast continental  
203 shelf since the late Miocene<sup>15</sup>, coincident with significant global climate, carbon and  
204 hydrologic cycle reorganizations<sup>4,13</sup>, continent-wide ice sheet expansion and  
205 stabilization<sup>7,8,13</sup>, Antarctic Circumpolar Current intensification, Southern Ocean cooling,  
206 and modern meridional thermal gradient development (Fig. 3b)<sup>1,13</sup>. Atmospheric cooling  
207 likely limited the amount of regional surface ablation, resulting in ice expansion and  
208 reduced surface-derived meltwater in the ASB catchment. Although open marine  
209 conditions intermittently existed on the shelf, the relative MS-III thickness and patterns  
210 of erosion within the ASB catchment suggest maximum grounding line retreat of  $\sim 150$   
211 kilometers<sup>15</sup> from its present location since the late Miocene. Thus, in contrast to the

212 adjacent Wilkes Subglacial Basin<sup>14</sup>, the ASB did not contribute significantly to sea level  
213 rise during Pliocene warmth<sup>15,16</sup>.  
214  
215 Sabrina Coast shelf records reveal the importance of atmospheric temperatures and  
216 surface-derived meltwater to Antarctica's ice mass balance. Although deeper, more  
217 continuous sampling of these sediments is required to assess the timing, magnitude, and  
218 rates of EAIS evolution in the ASB, the ice-proximal Sabrina Coast shelf record confirms  
219 model predictions of the region's long-term sensitivity to climate<sup>10,11,15,25,26</sup>. Critical for  
220 future global sea level rise scenarios is the potential for ASB catchment glaciers to revert  
221 from the extensive polar system of the last ~7 Ma to the surface meltwater-rich sub-polar  
222 system of the Oligo-Miocene (Fig. 3a), when average global temperatures and  
223 atmospheric CO<sub>2</sub> concentrations were similar to those anticipated under current warming  
224 projections (Figs. 3b-c)<sup>10,11,17</sup>. Presently, the Totten Glacier is thinning faster than any  
225 other East Antarctic outlet glacier<sup>11,27,28</sup> due to ocean thermal forcing<sup>28</sup>. Our findings  
226 suggest that ice in the ASB catchment may respond dramatically to anthropogenic  
227 climate forcing if regional atmospheric warming results in surface meltwater production.

228

## 229 **References**

230

- 231 1. Kennett J.P. Cenozoic evolution of Antarctic glaciation, the circum-Antarctic  
232 ocean, and their impact on global paleoceanography. *J. Geophys. Res.* **82**, 3843-  
233 3860 (1977).  
234
- 235 2. Coxall, H.K. et al. 2005. Rapid stepwise onset of Antarctic glaciation and deeper  
236 calcite compensation in the Pacific Ocean. *Nature* **433**, 53-57 (2005).  
237
- 238 3. Kominz, M.A., Browning, J.V., Miller, K.G., Sugarman, P.J., Mizintseva, S. &  
239 Scotese, C.R. Late Cretaceous to Miocene sea-level estimates from the New  
240 Jersey and Delaware coastal plain coreholes: An error analysis. *Basin Research*

- 241           **20**, 211-226 (2008).  
242
- 243           4. Mudelsee, M., Bickert, T., Lear, C.H. & Lohmann, G. Cenozoic climate changes:  
244           A review based on time series analysis of marine benthic  $\delta^{18}\text{O}$  records. *Rev.*  
245           *Geophys.* **52**, 333-374 (2014).  
246
- 247           5. Naish, T.R. *et al.* Orbitally induced oscillations in the East Antarctic ice sheet at  
248           the Oligocene/Miocene boundary. *Nature* **413**, 719-723 (2001).  
249
- 250           6. Naish, T.R. *et al.* Obliquity-paced Pliocene West Antarctic ice sheet oscillations.  
251           *Nature* **458**, 322-328 (2009).  
252
- 253           7. Cooper, A.K. *et al.* Cenozoic climate history from seismic reflection and drilling  
254           studies on the Antarctic Continental Margin. *In: Florindo, F., Siebert, M. (Eds.),*  
255           *Antarctic Climate Evolution. Developments in Earth and Environmental Sciences.*  
256           Elsevier, pp. 115-228 (2009).  
257
- 258           8. Escutia, C., Brinkhuis, H., Klaus, A. & Expedition 318 Scientists. Proc. Integrated  
259           Ocean Drilling Program 318 (Ocean Drilling Program Management International,  
260           Tokyo) (2011).  
261
- 262           9. Fretwell, P. *et al.* Bedmap2: improved ice bed, surface and thickness datasets for  
263           Antarctica. *Cryosphere* **7**, 375-393 (2013).  
264
- 265           10. Golledge, N.R. *et al.* The multi-millennial Antarctic commitment to future sea-  
266           level rise. *Nature* **526**, 421-425, (2015).  
267
- 268           11. DeConto, R.M. & Pollard, D. Contribution of Antarctica to past and future sea-  
269           level rise. *Nature* **531**, 591-597 (2016).  
270
- 271           12. Kehew, A.E., Piotrowski, J.A. & Jørgensen, F. Tunnel valleys: Concepts and  
272           controversies – A review. *Earth-Sci. Rev.* **113**, 33-58 (2012).  
273
- 274           13. Herbert, T.D. *et al.* Late Miocene global cooling and the rise of modern  
275           ecosystems. *Nat. Geosci.* **9**, 843-847 (2016).  
276
- 277           14. Cook, C.P. *et al.* Dynamic behavior of the East Antarctic ice sheet during  
278           Pliocene warmth. *Nat. Geosci.* **6**, 765-769 (2013).  
279
- 280           15. Aitken, A.R.A. *et al.* Repeated large-scale retreat and advance of Totten Glacier  
281           indicated by inland bed erosion. *Nature* **533**, 385-389 (2016).  
282
- 283           16. Rovere, A. *et al.* The Mid-Pliocene sea-level conundrum: Glacial isostasy,  
284           eustasy, and dynamic topography. *Earth Planet. Sci. Lett.* **387**, 27-33 (2014).  
285
- 286           17. Masson-Delmotte V. *et al.* Information from paleoclimate archives. *In* Climate

- 287 Change 2013: The Physical Science Basis. Contribution of Working Group I to  
288 the Fifth Assessment Report of the Intergovernmental Panel on Climate Change  
289 (T.F. Stocker *et al.* (eds.), pp. 383–464. Cambridge, UK: Cambridge University  
290 Press (2013).  
291
- 292 18. Anagnostou, E. *et al.* Changing atmospheric CO<sub>2</sub> concentration was the primary  
293 driver of early Cenozoic climate. *Nature* **533**, 380-384 (2016).  
294
- 295 19. DeConto, R.M. & Pollard, D. Rapid Cenozoic glaciation of Antarctica induced by  
296 declining atmospheric CO<sub>2</sub>. *Nature* **421**, 245-249 (2003).  
297
- 298 20. Pälike H. *et al.* The heartbeat of the Oligocene climate system. *Science* **314**, 1894-  
299 1898 (2006).  
300
- 301 21. Liebrand, D. *et al.* Evolution of the early Antarctic ice ages. *Proc. Natl. Acad. Sci.*  
302 *USA* **114**, 3867-3872 (2017).  
303
- 304 22. Scher, H.D., Bohaty, S.M., Smith, B.W. & Munn, G.H. Isotopic interrogation of a  
305 suspected late Eocene glaciation. *Paleoceanography* **29**, 628-644 (2014).  
306
- 307 23. Carter, A., Riley, T.R., Hillenbrand, C-D. & Rittner, M. Widespread Antarctic  
308 glaciation during the late Eocene. *Earth Planet. Sci. Lett.* **458**, 49-57 (2017).  
309
- 310 24. Passchier, S., Ciarletta, D.J., Miriagos, T.E., Bijl, P.K. & Bohaty, S.M. An  
311 Antarctic stratigraphic record of stepwise ice growth through the Eocene-  
312 Oligocene transition. *GSA Bull.* **129**, 318-330 (2017).  
313
- 314 25. Golledge, N.R., Levy, R.H., McKay, R.M., & Naish, T.R. East Antarctic ice sheet  
315 most vulnerable to Weddell Sea warming. *Geophys. Res. Lett.* **44**, 2343-2351  
316 (2017).  
317
- 318 26. Young, D.A. *et al.* A dynamic early East Antarctic Ice Sheet suggested by ice-  
319 covered fjord landscapes. *Nature* **474**, 72-75 (2011).  
320
- 321 27. Li, X., Rignot, E., Mouginot, J., & Scheuchl, B. Ice flow dynamics and mass loss  
322 of Totten Glacier, East Antarctica, from 1989 to 2015. *Geophys. Res. Lett.* **43**,  
323 6366–6373 (2016).  
324
- 325 28. Rintoul, S.R. *et al.* Ocean heat drives rapid basal melt of the Totten Ice Shelf. *Sci.*  
326 *Adv.* **2**, e1601610 (2016).  
327
- 328 29. Wright, A.P. *et al.* Evidence of a hydrological connection between the ice divide  
329 and ice sheet margin in the Aurora Subglacial Basin, East Antarctica. *J. Geophys.*  
330 *Res.* **117**, F01033, doi: 10.1029/2011JF002066 (2012).  
331
- 332 30. Close, D.I., Stagg, H.M.J & O'Brien, P.E. Seismic stratigraphy and sediment

333 distribution on the Wilkes Land and Terre Adélie margins, East Antarctica. *Mar.*  
334 *Geol.* **239**, 33-57 (2007).  
335

336 **Supplementary Information** is available in the online version of this paper.

337

338 **Acknowledgements** We thank the NBP14-02 science party, ECO captain and crew, and  
339 ASC technical staff aboard the *RV/IB N.B. Palmer*. NBP14-02 was supported by the  
340 National Science Foundation (NSF PLR-1143836, -1143837, -1143843, -1430550, and  
341 -1048343) and a GSA graduate student research grant to C. Smith. We thank the  
342 Antarctic Marine Geology Research Facility staff at Florida State University for sampling  
343 assistance and E. Thomas, M. Katz, F. Sangiorni, P. Bijl, and S. Manchester for  
344 discussions. This is UTIG Contribution #3137.

345

346 **Author Contributions** S.G. and A.S. contributed equally to this work, co-writing the  
347 manuscript with input from all authors. D.B., S.G., A.L., and A.S. conceived the study.  
348 B.F, R.F., S.G., A.L., A.S., C.S., and the shipboard scientific party collected geophysical  
349 data and samples on USAP cruise NBP14-02. All authors contributed to the analyses and  
350 interpretation of the results.

351

352 **Author Information** Reprints and permissions information is available at  
353 [www.nature.com/reprints](http://www.nature.com/reprints). The authors declare no competing financial interests. Readers  
354 are welcome to comment on the online version of the paper. Correspondence and requests  
355 for materials should be addressed to S.G. ([sean@ig.utexas.edu](mailto:sean@ig.utexas.edu)).

356

357 **Figure Captions**

358 **Figure 1| Aurora Subglacial Basin elevations and Sabrina Coast bathymetry. a,**  
359 Aurora Subglacial Basin (ASB) elevations<sup>9</sup> and Sabrina Coast shelf study location (black  
360 box; NBP14-02 (yellow) and published (white)<sup>30</sup> seismic lines indicated). Inset: ASB  
361 location (black box), Antarctica. ASB highlands (brown), reduced ice glacial pathways  
362 (white arrows)<sup>26</sup>, approximate retreated Oligo-Miocene (solid line) and late Miocene-  
363 Pleistocene (dashed line) grounding line locations<sup>15</sup>. **b,** NBP14-02 seismics, bathymetry,  
364 and BEDMAP2 bathymetry<sup>9</sup>; interpreted seismic lines (red) and jumbo piston cores (JPC;  
365 white) indicated. Inset: Regional bathymetry<sup>9</sup> and seismics. Sabrina Coast coastline,  
366 Moscow University Ice Shelf (MUIS), and shelf break indicated.

367

368 **Figure 2| Sabrina Coast seismic and piston core biostratigraphy. a,** Seismic line 17  
369 with cores in Megasequence I (MS-I, pre- to pro-glacial (gray shading)). MS-II  
370 (meltwater-rich glacial) overlies first expression of grounded ice (dark blue horizon).  
371 MS-III (glacial) overlies regional unconformity (light blue horizon). **b,** Biostratigraphy  
372 for JPC-55, based on pollen and benthic foraminifers (late Paleocene; brown shading),  
373 and JPC-54, based on pollen (early-to-middle Eocene; beige shading). **c,** Seismic line 13  
374 with cores relative to regional unconformity (light blue horizon). **d,** JPC-30 and -31  
375 diatom biostratigraphy, with conservative (beige shading, red line) and preferred (brown  
376 shading, blue line) ages.

377

378 **Figure 3| Composite Sabrina Coast section with glacial surfaces and climate**  
379 **indicators. a,** Composite seismic line with pre- to pro-glacial Megasequence I (MS-I;

380 black), glacial MS-II with erosion surfaces (initial: dark blue; subsequent: gray) overlain  
381 by a non-glacial interval and regional unconformity (light blue), and polar glacial MS-III.  
382 **b**, Cenozoic atmospheric CO<sub>2</sub> reconstructions<sup>17,18</sup> with 2 standard deviation error bars  
383 (black). **c**, Composite high-latitude benthic foraminifer δ<sup>18</sup>O record with blue uncertainty  
384 band generated/calculated as per [4], reflecting global ice volume and deep ocean  
385 temperatures<sup>4</sup>; **d**, New Jersey margin sea-level lowstands (black) with minimum  
386 uncertainty (grey envelope) and best estimates (blue line)<sup>3</sup>.

387

## 388 **METHODS**

### 389 **Seismic Data Acquisition, Processing, and Interpretation**

390 The 750 km of 3-m resolution multichannel seismic data were acquired using dual  
391 45 in<sup>3</sup> generator-injector (GI) guns and a 75-m long, 24-channel streamer in 2014 in  
392 heavy ice conditions aboard the *RV/IB N. B. Palmer*. Data processing followed standard  
393 steps of filtering, spherical divergence correction, normal moveout correction, and  
394 muting, but no deconvolution was required due to the quality of the GI source. All  
395 sediment thicknesses are presented in meters and based on a velocity of 2250 m/s;  
396 seafloor depths are based on a velocity of 1500 m/s. Acoustic basement is the limit of our  
397 reflectivity and interpreted as crystalline rock.

398 Seismic megasequences were identified based upon the presence or absence of  
399 erosional surfaces and seismic facies of the mappable units within the sediment packages.  
400 Seismic facies observed include: 1) stratified (laminated) or semi-stratified intervals  
401 interpreted as open marine, 2) relatively continuous layers with variable reflectivity  
402 interpreted as open marine conditions influenced by ice-rafting, and 3) chaotic,

403 discontinuous or transparent intervals interpreted as glacial to periglacial conditions. MS-  
404 I exhibits stratified, semi-stratified, and variably reflective (grey shading) intervals. MS-  
405 II exhibits chaotic and discontinuous intervals related to erosive surfaces, stratified or  
406 semi-stratified intervals, and prograding intervals. Rough, undulatory surfaces are  
407 indicators of glacial advance on continental shelves<sup>31</sup>. MS-III consists of chaotic or  
408 acoustically transparent intervals with thin intervals of stratified facies. The thickness of  
409 stratified intervals between erosional surfaces may be a proxy for duration of open water  
410 conditions and/or extent of ice retreat (and thus time/distance for readvance)<sup>32</sup>. Thus, MS-  
411 II includes extensive and/or long-lasting glacial retreats whereas MS-III records localized  
412 or relatively short-lived retreats.

413 All identified horizons are regionally mappable within the seismic survey area.  
414 Glacial erosion surfaces are interpreted based on roughness, extent of down-cutting, and  
415 association with overlying chaotic or discontinuous facies. Tunnel valley determinations  
416 are based on comparisons with imaged tunnel valleys from the North Sea, Alaska, and  
417 Svalbard<sup>32-38</sup>. Hydrologic modeling suggests tunnel valleys only form when meltwater  
418 exceeds the capacity of flow through porous glacial substrate and any sheet flow at the  
419 base of a glacier<sup>39</sup>. As tunnel valley size is expected to relate to discharge of subglacial  
420 meltwater, Sabrina Coast glacial erosion surfaces 3-5 and 8-9 are interpreted as  
421 meltwater-rich glaciations that likely required surface-derived meltwater. In the Ross Sea,  
422 a widespread regional unconformity that separates prograding shelf strata from glacial  
423 tills was interpreted to indicate widespread ice sheet expansion and the onset of ice  
424 loading, as suggested for the Sabrina Coast angular unconformity underlying MS-III<sup>40</sup>.  
425 Uninterpreted versions of the seismic profiles in Figs. 2a, c and 3a, including individual



426 lines from the regionally representative cross-shelf composite line (Fig. 3a), are included  
427 as Extended Data (Extended Data Fig. 1).

428

### 429 **Marine sediment collection, description, and physical properties analyses**

430 Marine sediments were collected in 440 to 550 meters of water 100-150 km  
431 offshore, on the Sabrina Coast continental shelf (Extended Data Table 1). Geophysical  
432 data guided the recovery of a suite of four <2 m long jumbo piston cores (JPCs) that  
433 targeted outcropping reflectors on the continental shelf (Figs. 1b, 2a, 2c, Extended Data  
434 Figs. 2-4). Seismic data, lithology, benthic foraminifers, diatoms, and bulk sediment  
435 geochemistry confirm that these sequences were deposited in open marine to subglacial  
436 settings. Sediment cores were transported (unsplit and at 4°C) to the Antarctic Marine  
437 Geological Research Facility at Florida State University, where they were split,  
438 photographed, visually described, x-rayed, and GEOTEK Multi-sensor Core Logger  
439 (MSCL) data were collected following standard protocols. The radiographs were  
440 interpreted in Adobe Photoshop with the contrast adjusted for each image. Organic  
441 carbon,  $\delta^{13}\text{C}$ , and  $\delta^{15}\text{N}$  analyses of bulk sediments were conducted using a Carlo Erba  
442 2500 Elemental Analyzer coupled to a continuous flow ThermoFinnigan Delta Plus XL  
443 IRMS at USF CMS following standard methods. Lithologic, physical properties, and  
444 geochemical data are shown in Extended Data Figures 2-4 and provided in  
445 Supplementary Information (SI).

446 Core JPC-55 (1.69 m) contains two distinct lithologic units (Extended Data Fig.  
447 2b). The upper unit (0-0.4 m; Unit 1) consists of Quaternary-recent diatom-rich sandy silt  
448 with relatively high magnetic susceptibility (SI) overlying a more consolidated lower unit

449 (0.4-1.69 m; Unit 2) of homogenous black micaceous silty fine sands with organic  
450 detritus, rare pyrite nodules, macro- and microfossils, and a ~10 cm diameter spherical  
451 siderite concretion nucleated around a monocot stem (Extended Data Figs. 2b, d, e; SI).

452 Core JPC-54 (1.21m), collected above the youngest clinoform, contains two  
453 distinct lithologic units (Fig. 2a, Extended Data Fig. 3b). The lithology of the upper unit  
454 (0-0.2 m; Unit 1) in JPC-54 is similar to that of JPC-55 and overlies a lower unit (0.2-  
455 1.21 m; Unit 2) composed of structureless gravel-rich sandy silts to silty coarse sands  
456 with centimeter-scale angular limestones throughout Units 1 and 2 (Extended Data Fig.  
457 3b). A conservative approach to ice-rafted debris (IRD) interpretation was undertaken in  
458 these sediments and only angular limestones  $\geq 1$  cm were interpreted as IRD. Lighter  
459 colored sediment with modern diatoms, visible on the right-hand side of JPC-54,  
460 indicates flow-in below ~80 cm, likely due to a partial piston stroke; flowage of dark  
461 sediment along the right side of the upper core is consistent with this interpretation and/or  
462 on-deck or transport disturbance (Extended Data Fig. 3b). However, angular limestones  
463 are observed throughout and a majority are surrounded by the dark colored sediments.

464 Core JPC-30 (0.52 m plus cutter nose) contains diatom-bearing sandy muds, with  
465 intervals of well-sorted sands (0-0.25 m). Sub-angular diatomite clasts are present in a  
466 mud matrix between 0.25 and 0.52 m. In the core cutter nose, we recovered stratified  
467 diatomite and gravelly diatom-bearing sandstone and sandy diatomite above a sharp  
468 contact with sandy diamictite below (Extended Data Fig. 4b).

469 Core JPC-31 (0.47 m) contains an upper unit of muddy diamicton (0-0.29 m).  
470 Between 0.29 and 0.47 m, angular diatomite clasts are present, which may have been  
471 fractured during coring (Extended Data Fig. 4c).

472

473 **Biostratigraphic methods**

474 *Palynology*: Nine samples from JPC-54 and eight samples from JPC-55  
475 (Extended Data Figs. 2b, 3b, Extended Data Table 2) were processed at Global Geolab  
476 Limited, Alberta, Canada using palynological techniques suited for Antarctic sediments.  
477 Approximately five grams of dried sediment were weighed and spiked with a known  
478 quantity of *Lycopodium* spores to allow computation of palynomorph concentrations.  
479 Acid soluble minerals (carbonates and silicates) were removed via digestion in HCl and  
480 HF acids. Residues were concentrated by filtration through a 10- $\mu$ m sieve and mounted  
481 on microscope slides for analyses. Analysis was conducted under 100x oil immersion  
482 objective with a Zeiss Axio microscope. For samples with sufficient palynomorph  
483 abundance, a minimum of 300 palynomorphs were tabulated per sample. For samples  
484 with low abundance, the entire residue was tabulated. A database of all palynomorphs  
485 recovered was prepared and key species were photographically documented. The  
486 taxonomic evaluation was completed based on the type specimen repository and library at  
487 the Louisiana State University Center for Excellence in Palynology (CENEX).  
488 Palynological results are presented in Extended Data Table 2.

489 *Benthic Foraminifera*: Benthic foraminifer counts and biostratigraphic data were  
490 generated for 16 depths in JPC-55 and five depths in JPC-54 using standard protocols  
491 (Extended Data Figs. 2b, 5, Extended Data Table 3). Sediment samples between 20 and  
492 30cc were washed over a 63- $\mu$ m sieve with deionized water. Sample residues were dried  
493 at 50°C for 24 hours, transferred to labeled vials, dry sieved into 250- and 150- $\mu$ m  
494 fractions, and examined using a Zeiss Stemi 2000-C stereomicroscope with a 1.6X lens

495 and 10X eyepiece (Magnification: 10.4-80X). Genus and species identifications were  
496 refined using Scanning Electron Microscopy (SEM) at the University of South Florida  
497 College of Marine Science (Extended Data Fig. 5). All benthic foraminifer individuals  
498 present in each JPC-55 sample are tabulated in Extended Data Table 3. In JPC-55,  
499 preservation of aragonite and calcium carbonate tests, determined both visually and via  
500 SEM, ranges from poor to excellent (Extended Data Fig. 5). Five species of well-  
501 preserved aragonitic and calcareous benthic foraminifers were observed throughout JPC-  
502 55 Unit 2 (ED Table 3). No foraminifers were observed in JPC-54.

503 *Diatoms:* Diatom biostratigraphy was conducted on two sets of NBP14-02  
504 samples: 1) JPC-30 cutter nose diatomites and 2) diatomite clasts from the bottom of  
505 JPC-31 (Extended Data Figs. 4b, 4d, 6). Quantitative slides were prepared at Colgate  
506 University for diatom assemblage studies and biostratigraphic evaluation using a settling  
507 technique that results in a random and even distribution of frustules<sup>41</sup>; sub-samples were  
508 sieved at 10- and 63- $\mu$ m to concentrate unbroken frustules for examination. Photographic  
509 documentation at 1000x magnification using oil immersion on Olympus BX50 and BX60  
510 microscopes was completed at Colgate University (Extended Data Fig. 6). The beige  
511 shading in Fig. 2d represents the conservative zonal assignment and age range, whereas  
512 the brown shading represents the refined age interpretation. Age constraints for key  
513 diatom bioevents are derived from the statistical compilation and analysis of average age  
514 ranges for Southern Ocean taxa<sup>42</sup>.

515

## 516 **Chronology**

517 *Palynological biostratigraphic zonation scheme:* Palynological biostratigraphic  
518 zonation of cores NBP14-02 JPC-54 and JPC-55 is based on the presence of a few key  
519 species and limited data available from Antarctica and surrounding regions (e.g. Australia  
520 and New Zealand). *Gambierina edwardsii* and *Gambierina rudata* are known as  
521 Cretaceous to Paleocene species. A recent study published a robust LAD for these species  
522 at the Paleocene/Eocene boundary on the East Tasman Rise (ODP Site 1172)<sup>43</sup>. However,  
523 in southeastern Australia, the two *Gambierina* species observed in the Sabrina Coast  
524 sequence range into the earliest early Eocene<sup>44</sup>. Extended ranges for the *Gambierina* sp.  
525 (dashed lines; Fig. 2b) are based on the palynological analysis of ODP Site 1166 in Prydz  
526 Bay<sup>45,46</sup>, where abundant well-preserved *Gambierina* specimens were observed and not  
527 considered reworked. Consequently, those authors extended the *Gambierina* sp. range  
528 into the early-to-middle Eocene in East Antarctica<sup>45,46</sup>.

529 *Microalatidites paleogenicus* has a Paleogene to Neogene range<sup>46</sup>. Although we  
530 are adopting their range herein, there is some controversy with this range. The first  
531 occurrence of *Microalatidites paleogenicus* is listed as Senonian in Australia and New  
532 Zealand<sup>47</sup>, but there is no robust evidence supporting an extended range in Antarctica. In  
533 Fossilworks (PaleoDB taxon number: 321781), *Microalatidites paleogenicus* is listed as  
534 having a range from 55.8 to 11.608 Ma.

535 *Nothofagidites lachlaniae* ranges from Paleogene to modern while *Nothofagidites*  
536 *flemingii-rocaensis* ranges from Paleogene to Neogene<sup>46</sup>. The range for *N. lachlaniae* in  
537 New Zealand is listed as Late Cretaceous to present and is similar to other forms<sup>48</sup>. In the  
538 Paleocene and Eocene, there is climatically-induced variability observed in the  
539 *Nothofagidites* ranges. For example, broad regional vegetation changes (e.g. the

540 abundance of *Nothofagidites lachlaniae* in western Southland (Ohai, Waiau and Balleny  
541 basins) and its scarcity in other Eocene sections (Waikato, the Taranaki basin, and the  
542 west coast of New Zealand's South Island) may be related to paleoenvironmental  
543 factors<sup>49</sup>. The type material is Pliocene<sup>50</sup>, but the distinction of this species from other  
544 *Fuscospora* pollen (including *N. brachyspinulosa* and *N. waipawaensis*) is problematic.  
545 If *N. waipawaensis* and *N. senectus* are excluded, then the New Zealand FAD of other  
546 *Fuscospora* pollen would be late Paleocene.

547 In Southern Australia, the FAD of *N. flemingii* is in the upper part of the  
548 *Lygistepollenites balmei* Zone (late Paleocene)<sup>51,52</sup>. However, in a detailed study of  
549 Paleocene-Eocene transition strata in western Victoria, *N. flemingii* is not reported<sup>53</sup>. In  
550 New Zealand, the *N. flemingii* FAD is reported as middle Eocene<sup>54,55</sup>. However, in well-  
551 dated early Eocene New Zealand localities, occasional small *N. flemingii*-like specimens  
552 are observed; their identification is under debate. Due to the relative geographic  
553 proximity of East Antarctica and Southern Australia in the Paleogene, we follow [52, 53]  
554 and place the FADs of both species in the late Paleocene.

555 *Proteacidites tenuiexinus* has a range from 66.043 to 15.97 Ma (PaleoDB taxon  
556 number: 277519 at fossilworks.org). We adopt the published late Paleocene *Proteacidites*  
557 *tenuiexinus* FAD in Southeastern Australia<sup>51</sup>, but acknowledge that the FAD could be as  
558 early as early Paleocene.

559 Two pollen species present in core JPC-54 were not observed in core JPC-55,  
560 *Nothofagidites cranwelliae* and *Nothofagidites emarcidus*. Most verified references for  
561 *Nothofagidites cranwelliae* and *Nothofagidites emarcidus* (e.g. those with specimens  
562 properly identified; the *Nothofagidites* group is diverse, complex, and easily

563 misidentified) place the FAD of both of these species in the early Eocene, at the  
564 earliest<sup>56,57</sup>. The latter species was also found in the Eocene of Western Australia<sup>58</sup>.

565 *Diatom preservation and biostratigraphy:* The diatom assemblages present in  
566 cores JPC-30 and JPC-31 are indistinguishable, although preservation is better and  
567 abundance higher in the JPC-31 diatomites compared to the sandy diatom muds  
568 recovered in JPC-30. Overall, preservation is moderate to good in JPC-31 and poor to  
569 moderate in JPC-30 (Extended Data Fig. 6). Diatoms in both cores suffer from a high  
570 degree of fragmentation. Large centric taxa, such as *Actinocyclus* spp. and *Thalassiosira*  
571 spp., are generally broken, whereas the smaller centric and pennate specimens are well  
572 preserved (Extended Data Fig. 6). *Denticulopsis* specimens are generally well preserved,  
573 although though the longer specimens of *D. delicata* are typically broken. *Rouxia* spp.  
574 occur mostly in fragments making identification more problematic. Similarly, specimens  
575 of *Fragilariopsis* spp. are dominantly present as broken specimens, with the exception of  
576 a few *F. praecurta* specimens (Extended Data Fig. 6).

577 Many of the diatom species present in both JPC-30 and JPC-31 have long age  
578 ranges and do not provide good biostratigraphic age constraints (e.g., *Coscinodiscus*  
579 *marginatus*, *Trinacria excavata*). However, the presence of several common taxa  
580 provides robust support for a late Miocene-earliest Pliocene age. These taxa include:  
581 *Actinocyclus ingens* var. *ovalis*, *Denticulopsis delicata*, *Fragilariopsis praecurta*,  
582 *Thalassiosira oliverana* var. *sparsa*, *Thalassiosira torokina* (large form), and  
583 silicoflagellates in the *Distephanus speculum speculum* 'pseudofibula plexus' group.  
584 There is very little evidence of reworking of older material, with only one specimen of  
585 *Pyxilla* sp. and a fragment of *Hemiaulus* sp. observed; all species within both of these

586 genera are typical of the Eocene and Oligocene.

587 *Age determination for JPC-55 sediments:* Based on our conservative pollen  
588 zonation scheme, we favor a late Paleocene to earliest early Eocene age for the  
589 exceptionally diverse JPC-55 *in situ* fossil pollen assemblage; this assemblage is easily  
590 distinguishable from reworked Cretaceous microfossils present in the sediments (Fig. 2b).  
591 The presence of middle bathyal benthic foraminifer species *Gyroidinoides globosus* and  
592 *Palmula* sp., both of which went extinct at the Paleocene-Eocene boundary<sup>59</sup>, enables us  
593 to further refine the pollen-based age designation to late Paleocene (Extended Data Fig.  
594 5). Although its first occurrence may be diachronous, the presence of aragonitic Cenozoic  
595 benthic foraminifer species *Hoeglundina elegans*<sup>59-63</sup> indicates that these sediments are  
596 Cenozoic in age, confirming the interpretation that co-occurring Cretaceous microfossils  
597 are reworked. *H. elegans* and other aragonitic benthic foraminifers are most common in  
598 upper to middle bathyal assemblages along the southern Australian margin and the  
599 Australo-Antarctic Gulf during the Paleocene and Eocene<sup>60,63</sup>. Thus, we conservatively  
600 designate an age of late Paleocene to sediments in the lower unit (Unit 2) of JPC-55 (Fig.  
601 2b, Extended Data Fig. 2b).

602 *Age determination for JPC-54 sediments:* Pollen bistratigraphy constrains the  
603 depositional age of JPC-54 Unit 2 sediments to the early-to-middle Eocene (Fig. 2b,  
604 Extended Data Fig. 3b). No foraminifers are observed in the lower lithologic unit of JPC-  
605 54. Thus, based on the pollen assemblage alone, we favor an early-to-middle Eocene age  
606 for sediments in the lower unit (Unit 2) of JPC-54.

607 *Age determination for JPC-30 and JPC-31 sediments:* Based on Southern Ocean  
608 diatom ages<sup>42</sup>, the FAD of *T. oliverana* var. *sparsa* (8.61 Ma) and the LAD of *T. ingens*



609 var. *ovalis* (4.78 Ma) provide a conservative age estimate for the diatom assemblages  
610 present in JPC-30 and JPC-31 (8.61–4.78 Ma; Fig. 2d). A more restricted age  
611 interpretation is possible if the presence of *Shionodiscus tetraoestrupii* (FAD 6.91 Ma)  
612 and the absence of the typical early Pliocene taxon *Thalassiosira inura* (FAD 5.59 Ma)  
613 are considered, indicating an age between 6.91 and 5.59 Ma (Fig 2d). This more  
614 restricted age should be considered tentative, since precise calibrations for many  
615 Southern Ocean diatom bioevents in the Chron C3–C3A (4.2–7.1 Ma) interval are  
616 compromised by multiple short hiatuses at many drill sites and poor magnetostratigraphy.  
617 Further age refinement for the JPC-30 and JPC-31 samples is likely possible as diatom  
618 biostratigraphic data are published for expanded Late Neogene sections recovered on the  
619 Wilkes Land margin<sup>64</sup>. However, the more conservative age estimate (8.61–4.78 Ma; Fig.  
620 2d) is well supported by the presence of several taxa with well-calibrated ages in the  
621 Southern Ocean, including *Rouxia naviculoides* (FAD 9.84 Ma), *Thalassiosira oliverana*  
622 (FAD 9.73 Ma), and *Thalassiosira torokina* (FAD 9.36 Ma). The absence of  
623 *Denticulopsis dimorpha* (LAD 9.75 Ma), *Denticulopsis ovata* (LAD 8.13), *Thalassiosira*  
624 *complicata* (FAD 5.12 Ma), *Fragilariopsis barronii* (FAD 4.38 Ma), and *Fragilariopsis*  
625 *interfrigidaria* (FAD 4.13 Ma) support this age assessment.

626

627 **Data availability.** The seismic data from the study are available in the Academic Seismic  
628 Datacenter at the University of Texas Institute for Geophysics ([http://www-  
629 udc.ig.utexas.edu/sdc/cruise.php?cruiseIn=nbp1402](http://www-udc.ig.utexas.edu/sdc/cruise.php?cruiseIn=nbp1402)). Sediment cores are archived in the  
630 NSF-funded Antarctic Core Repository at Oregon State University. The authors declare  
631 that all other data that support the findings of this study are available within the paper and

632 its supplementary information files; these data may also be downloaded from the US  
633 Antarctic Program Data Center (USAP-DC; [www.usap-dc.org](http://www.usap-dc.org)).

634

635 **Methods References**

636

637 31. Anderson, J. & Bartek, L.R. Cenozoic glacial history of the Ross Sea revealed by  
638 intermediate resolution seismic reflection data combined with drill site  
639 information. pp. 213–263 in *The Antarctic Paleoenvironment: A Perspective on*  
640 *Global Change*. J.P. Kennett and D.A. Warnke, eds., *Antarctic Research Series*,  
641 vol. 56, American Geophysical Union (1992).

642

643 32. Ó’Cofaigh, C. Tunnel valley genesis. *Prog. Phys. Geog.* **20**, 1-19 (1996).

644

645 33. Huuse, M. & Lykke-Andersen, H. Over-deepened Quaternary valleys in the  
646 eastern Danish North Sea: morphology and origin. *Quat. Sci. Rev.* **19**,1233-1253  
647 (2000).

648

649 34. Denton, G.H. & Sugden, D.E. Meltwater features that suggest Miocene ice-sheet  
650 overriding of the Transantarctic Mountains in Victoria Land, Antarctica. *Geogr.*  
651 *Ann. A* **87**, 67-85 (2005).

652

653 35. Lonergan, L., Maidment, S. & Collier, J. Pleistocene subglacial tunnel valleys in  
654 the central North Sea basin: 3-D morphology and evolution. *J. Quat. Sci.* **21**, 891-  
655 903 (2006).

656

657 36. Elmore, C.R., Gulick, S.P.S., Willems, B., & Powell, R., Seismic stratigraphic  
658 evidence for glacial expanse during glacial maxima in the Yakutat Bay Region,  
659 Gulf of Alaska. *Geochem. Geophys. Geosys.* **14**, p. 1294-1311 (2013).

660

661 37. Van der Vegt, P., Janszen, A., & Moscariello, A. Tunnel valleys: current  
662 knowledge and future perspectives. *Geol. Soc. London Spec. Publ.* **368**, 75-97  
663 (2012).

664

665 38. Bjarnadóttir, L.R., Winsborrow, M.C.M., & Andreassen, K. Large subglacial  
666 meltwater features in the central Barents Sea. *Geology* **45**,159-162 (2017).

667

668 39. Piotrowski, J.A. Subglacial hydrology in north-western Germany during the last  
669 glaciation: Groundwater flow, tunnel valleys and hydrologic cycles. *Quat. Sci.*  
670 *Rev* **16**, 169-186 (1997).

671

672 40. Bart, P.J. Were West Antarctic Ice Sheet grounding events in the Ross Sea a  
673 consequence of East Antarctic Ice Sheet expansion during the middle Miocene?  
674 *Earth Planet. Sci. Lett.* **216**, 93-107 (2003).

- 675  
676 41. Scherer, R.P. A new method for the determination of absolute abundance of  
677 diatom and other silt-sized sedimentary particles. *J. Paleolimnology* **12**, 171-179  
678 (1994).  
679
- 680 42. Crampton, J.S. *et al.* Southern Ocean phytoplankton turnover in response to  
681 stepwise Antarctic cooling over the past 15 million years. *Proc. Natl. Acad. Sci.*  
682 *USA* **113**, 6868-6873 (2016).  
683
- 684 43. Contreras, L. *et al.* Southern high-latitude terrestrial climate change during the  
685 Paleocene–Eocene derived from a marine pollen record (ODP Site 1172, East  
686 Tasman Plateau). *Clim. Past Discuss.* **10**, 291-340 (2014).  
687
- 688 44. Partridge, A.D. Late Cretaceous–Cenozoic palynology zonation Gippsland Basin,  
689 Australian Mesozoic and Cenozoic palynology zonation—update to the 20004  
690 Geologic Time Scale, Geoscience Australia, Record 2006/23 (2006).  
691
- 692 45. MacPhail, M.K. & Truswell, E.M. Palynology of Site 1166, Prydz Bay, East  
693 Antarctica. In Cooper, A.K., O’Brien, P.E. & Richter, C. (Eds.), *Proc. ODP, Sci.*  
694 *Results* **188**, 1-43 (2004).  
695
- 696 46. Truswell, E.M. & MacPhail, M.K. Fossil forests on the edge of extinction: What  
697 does the fossil spore and pollen evidence from East Antarctica say? *Austral. Syst.*  
698 *Bot.* **22**, 57-106 (2009).  
699
- 700 47. Raine, J.I., Mildenhall, D.C. & Kennedy, E.M. New Zealand fossil spores and  
701 pollen: an illustrated catalogue. 4th edition. GNS Science Miscellaneous Series, 4,  
702 <http://data.gns.cri.nz/sporepollen/index.htm> (2011).  
703
- 704 48. Hill, R.S. (Ed.). History of the Australian vegetation: Cretaceous to Recent.  
705 Cambridge University Press (Cambridge). p. 233 (1994).  
706
- 707 49. Truswell, E. M. Recycled Cretaceous and Tertiary pollen and spores in Antarctic  
708 marine sediments: a catalogue. *Palaeontographica Abt. B* **186**, 121-174 (1983).  
709
- 710 50. Pocknall, D.T. Late Eocene to early Miocene vegetation and climate history of  
711 New Zealand, *J. R. Soc. N.Z.* **19**, 1-18 (1989).  
712
- 713 51. Dettmann, M.E., Pocknall, D.T., Romero, E.J. & Zamalao, M. del C.  
714 *Nothofagidites* Erdtman ex Potonie, 1960; a catalogue of species with notes on the  
715 paleogeographic distribution of *Nothofagus* BI. (Southern Beech). *N.Z. Geol. Sur.*  
716 *Paleo. Bull.* **60**, 1-79 (1990).  
717
- 718 52. Stover, L.E. & Partridge, A.D. Tertiary and Late Cretaceous spores and pollen  
719 from the Gippsland Basin, southeastern Australia. *Proc. Roy. Soc. Victoria* **85**,  
720 237-286 (1973).

- 721  
722 53. Stover, L.E. & Evans, P.R. Upper Cretaceous-Eocene spore-pollen zonation,  
723 offshore Gippsland Basin, Australia. *Geol. Soc. Australia Spec. Pub.* **4**, 55-72  
724 (1973).  
725  
726 54. Harris, W.K. Basal Tertiary microfloras from the Princetown area, Victoria,  
727 Australia. *Palaeontographica Abt. B* **115**, 75-106 (1965).  
728  
729 55. Couper, R.A. New Zealand Mesozoic and Cainozoic plant microfossils. *N.Z.*  
730 *Geol. Sur. Paleo. Bull.* **32**, 87 pages (1960).  
731  
732 56. Raine, J.I. Outline of a palynological zonation of Cretaceous to Paleogene  
733 terrestrial sediments in west coast region, South Island, New Zealand. *N.Z. Geol.*  
734 *Survey Rept.* **109**, 1-82 (1984).  
735  
736 57. Greenwood, D.R., Moss, P.T., Rowett, A.I., Vadala, A.J. & Keefe, R.L. Plant  
737 communities and climate change in southeastern Australia during the early  
738 Paleogene. *Geol. Soc. Spec. Pap.* **369**, 365-380 (2003).  
739  
740 58. Stover, L.E. & Partridge, A.D. Eocene spore-pollen from the Werillup Formation,  
741 Western Australia. *Palynology* **6**, 69-96 (1982).  
742  
743 59. Thomas, E. Late Cretaceous through Neogene deep-sea benthic foraminifers  
744 (Maud Rise, Weddell Sea, Antarctica). *Proc. ODP, Sci. Res.* **113**, 571-594 (1990).  
745  
746 60. McGowran, B. Two Paleocene foraminiferal faunas from the Wangerrip Group,  
747 Pebble Point Coastal section, Western Victoria. *Proc. Roy. Victoria* **79**, 9-74  
748 (1965).  
749  
750 61. Brotzen, F. The Swedish Paleocene and its Foraminiferal Fauna. *Arsbok Sveriges*  
751 *Geologiska Undersokning*, **42**, 1-140 (1948).  
752  
753 62. Holbourn, A., Henderson, A. & MacLeod, N. Atlas of Benthic Foraminifera.  
754 Wiley-Blackwell, London, England. 634 pp (2013).  
755  
756 63. Li, Q., James, N.P. & McGowran, B. Middle and late Eocene Great Australian  
757 Bight lithobiostratigraphy and stepwise evolution of the southern Australian  
758 continental margin. *Aus. J. Earth Sci.* **50**, 113-128 (2003).  
759  
760 64. Tauxe, L. *et al.* Chronostratigraphic framework for the IODP Expedition 318  
761 cores from the Wilkesland Margin: Constraints for paleoceanographic  
762 reconstruction. *Paleoceanography* **27**, PA2214, doi:10.1029/2012PA002308  
763 (2012).  
764

765 **Extended Data Legends**

766

767 **Extended Data Figure 1| Uninterpreted NBP14-02 seismic profiles with line**  
768 **crossings and coring sites indicated. a**, Line 13 with piston core sites JPC-30 and JPC-  
769 31 and formation penetration depths indicated by red lines. **b**, Line 17 with core sites  
770 JPC-55 and JPC-54 and formation penetration depths indicated by red lines. **c**, Line 07  
771 showing intersection with Line 10. **d**, Line 10 showing intersections with Line 07 and  
772 Line 21. **e**, Line 21 showing intersection with Line 10.

773

774 **Extended Data Figure 2| Site location and sedimentological, geochemical, and**  
775 **paleontological data from piston core NBP14-02 JPC-55 plotted versus depth. a**,  
776 CHIRP record of JPC-55 site; location and penetration indicated (red line); site  
777 coordinates and multibeam depth (MB) included. **b**, Gastropod steinkern (70-72 cm). **c**,  
778 Siderite concretion with monocot stem nucleus (118-125 cm). **d**, Close-up of monocot  
779 stem. **e**, JPC-55 lithologic unit, photograph, x-ray radiograph, graphic lithology, coring  
780 disturbance, sedimentary structures, lithologic accessories, sample locations, age, benthic  
781 foraminifers/30 cc sediment, magnetic susceptibility, GRA bulk density (grams/cc  
782 sediment), bulk sediment  $\delta^{13}\text{C}_{\text{org}}$  (per mil; VPDB‰), and Carbon/Nitrogen (C/N) plotted  
783 versus depth in centimeters below sea floor (cmbsf; SI).

784

785 **Extended Data Figure 3| Site location and sedimentological and geochemical data**  
786 **from piston core NBP14-02 JPC-54 plotted versus depth. a**, JPC-54 lithologic unit,  
787 photograph, x-ray radiograph, graphic lithology, coring disturbance, sedimentary  
788 structures, lithologic accessories, sample locations, age, magnetic susceptibility (SI),  
789 GRA bulk density (grams/cc sediment), and bulk sediment  $\delta^{13}\text{C}_{\text{org}}$  (per mil; VPDB‰)  
790 plotted versus depth in centimeters below sea floor (cmbsf). **b**, CHIRP record of JPC-54  
791 site; location and penetration indicated (red line); site coordinates and multibeam depth  
792 (MB) included.

793

794 **Extended Data Figure 4| Site location and sedimentological data from piston cores**  
795 **NBP14-02 JPC-30 and JPC-31 plotted versus depth. a**, CHIRP record of JPC-30 site;  
796 location and penetration indicated (red line); site coordinates and multibeam depth (MB)  
797 included. **b**, JPC-30 lithologic unit, photograph, x-ray radiograph, graphic lithology,  
798 coring disturbance, sedimentary structures, lithologic accessories, sample locations, age,  
799 magnetic susceptibility (SI), and GRA bulk density (grams/cc sediment) plotted versus  
800 depth in centimeters below sea floor (cmbsf). **c**, CHIRP record of JPC-31 site; location,  
801 and penetration indicated (red line). **d**, JPC-31 lithology, age, and physical properties as  
802 above.

803

804 **Extended Data Figure 5| Benthic foraminifers from piston core NBP14-02 JPC-55.**  
805 **a**, *Hoeglundina elegans* (76-78 cmbsf). **b**, SEM of *Hoeglundina elegans* (76-78 cmbsf).  
806 **c**, *Ceratobulimina* sp. (70-72 cmbsf). **d**, *Ceratobulimina* sp. (70-72 cmbsf). **e**, SEM of  
807 *Ceratobulimina* sp. (70-72 cmbsf). **f**, SEM of *Gyroidinoides globosus* (110-113 cmbsf).  
808 **g**, SEM of *Gyroidinoides globosus* (110-113 cmbsf). **h**, *Gyroidinoides globosus* with  
809 pyrite (136-138 cmbsf). **i**, *Gyroidinoides globosus* with zoom in of umbilicus; pyrite on  
810 lower right side of test (136-138 cmbsf). **j**, *Palmula* sp. (136-138 cmbsf; test >450  $\mu\text{m}$ ).

811

812 **Extended Data Figure 6| Siliceous microfossils from piston core NBP14-02 JPC-31**  
813 **diatomite sample. a, *Thalassiosira torokina*. b, *Thalassiosira oliverana* var. *sparsa*. c,**  
814 ***Actinocyclus ingens* var. *ovalis*. d, *Coscinodiscus marginatus*. e, *Azpeitia* sp. 1. f,**  
815 ***Actinocyclus* sp. g, *Actinocyclus* sp. h, *Shionodiscus tetraoestrupii*. i, *Shionodiscus***  
816 ***tetraoestrupii*. j, *Shionodiscus oestrupii*. k, *Denticulopsis delicate*. l, *Denticulopsis***  
817 ***simonsenii*/D. *vulgaris*. m, *Denticulopsis simonsenii*/D. *vulgaris*. n, *Denticulopsis***  
818 ***delicate*. o, *Denticulopsis simonsenii*/D. *vulgaris*. p, *Rouxia naviculoides*. q,**  
819 ***Fragilariopsis praecurta*. r, *Fragilariopsis* sp. 1. s, *Trinacria excavate*. t, *Rhizosolenia***  
820 ***hebetate*. u, *Eucampia antarctica* var. *recta*. v, *Distephanus speculum speculum* f.**  
821 ***varians*. Sample from 43-45 cmbsf.**  
822

823 **Extended Data Table 1| NBP14-02 piston core locations, water depths, and**  
824 **recovered core lengths.**

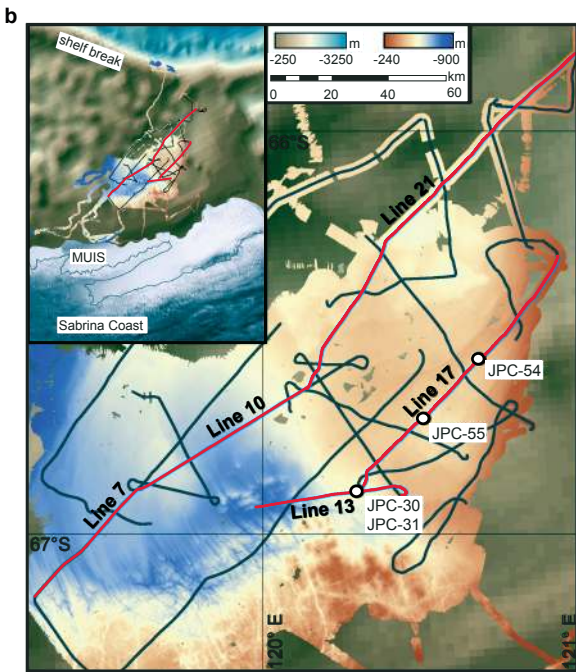
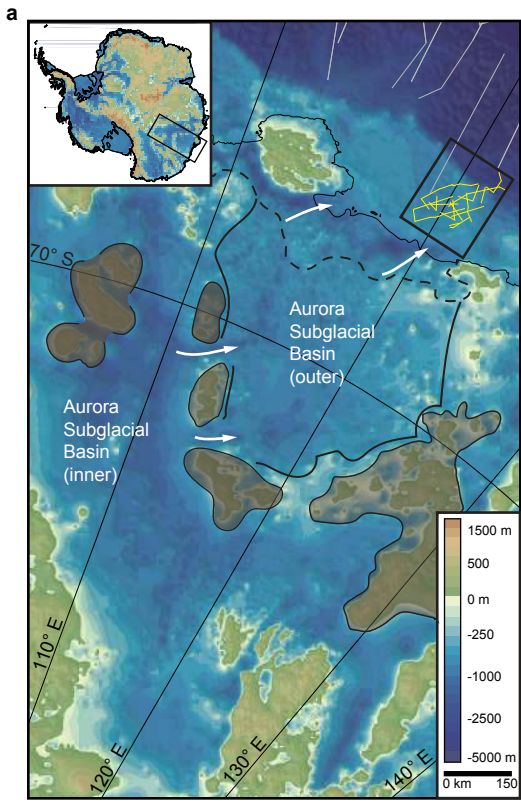
825

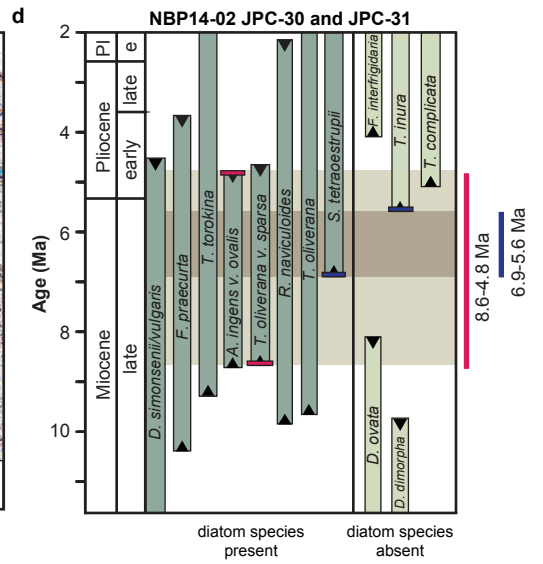
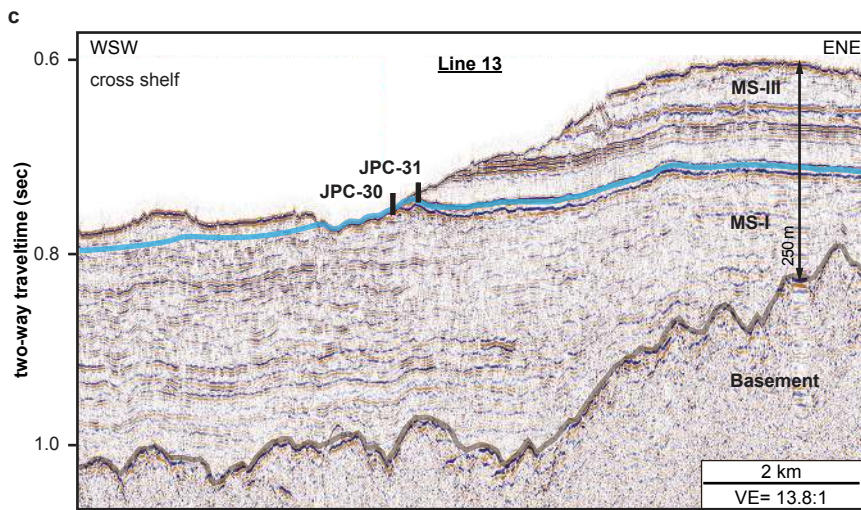
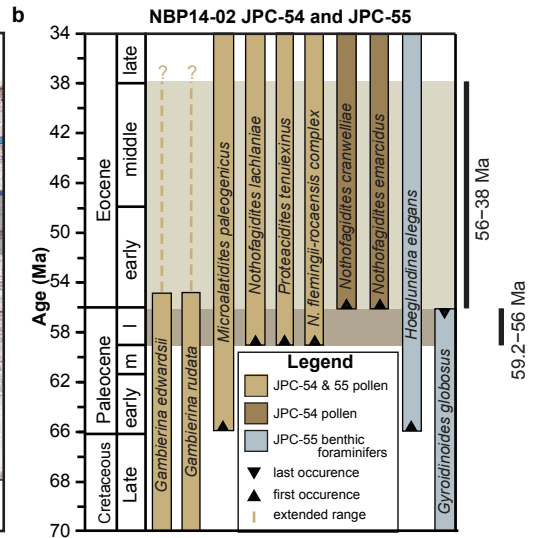
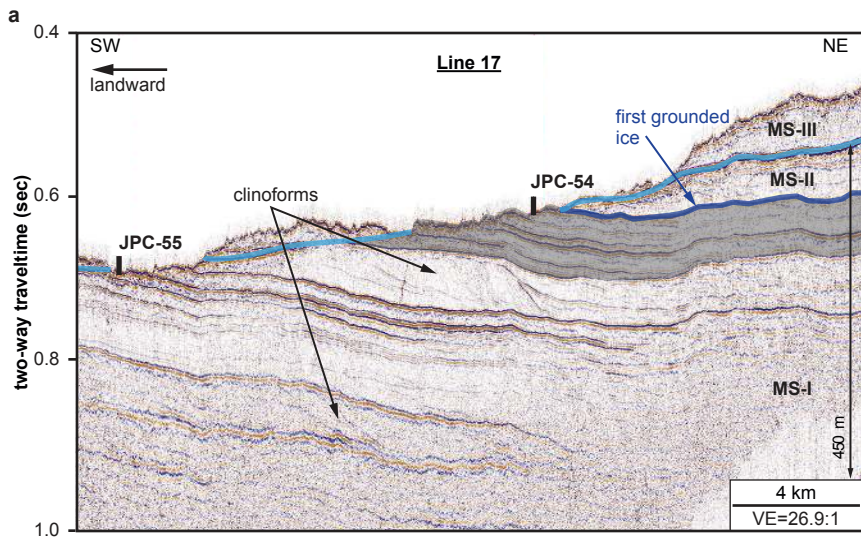
826 **Extended Data Table 2| Piston core NBP14-02 JPC-55 and JPC-54 raw terrestrial**  
827 **pollen counts.**

828

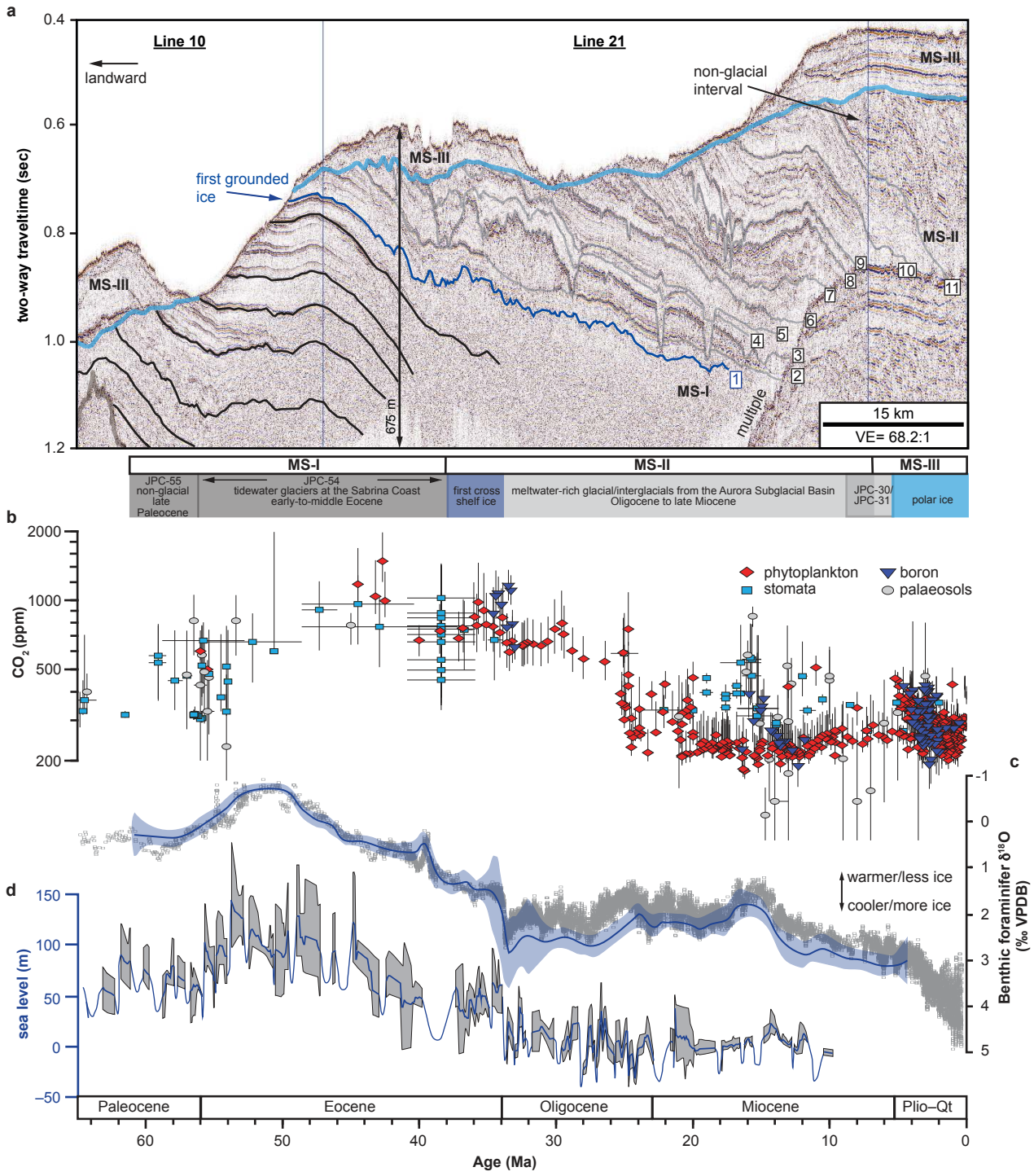
829 **Extended Data Table 3| Piston core NBP14-02 JPC-55 raw benthic foraminifer**  
830 **counts.**

831









Gulick et al\_Fig. 3